11th International Symposium on Magnetic Bearings
August 26-29, Nara, Japan

BASIC CHARACTERISTICS OF IMPROVED BEARINGLESS MOTOR WITH PASSIVE MAGNETIC BEARINGS

Yukiko Nakano, Tetsuro Asami, Junichi Asama, Akira Chiba, Tadashi Fukao
Dept. of Electrical Engineering, Fac. of Science and Technology,
Tokyo University of Science, Noda, Chiba 278-8510 Japan
chiba@rs.noda.tus.ac.jp

Takeshi Hoshino, Atsushi Nakajima
Japan Aerospace Exploration Agency (JAXA), Chofu, Tokyo 182-8522 Japan
nakajima@chofu.jaxa.jp

ABSTRACT

In this paper, basic characteristics of a bearingless motor with passive magnetic bearings (PMBs) are presented. A bearingless motor is actively controlled in two perpendicular radial movements, and is passively stable in the other three degrees of freedom, i.e., axial and conical movements. With PMBs, the stiffness is enhanced in axial and conical movements. To enhance stiffness, an improved machine has been designed. The experimental results of basic characteristics in the proposed machine are presented. The experimental results are compared to the calculated ones using three-dimensional finite element method (3D-FEM). The experimental results of the proposed machine with and without PMBs are compared. It is presented that a bearingless motor with PMBs has significantly enhanced the axial and conical stiffness.

INTRODUCTION

A bearingless motor is a single electric device combining a magnetic bearing and motoring functionality, thus a bearingless motor can suspend a rotating shaft without mechanical contact and generate torque [1-11]. The non-contact suspension is free from particles, maintenance free and possible high rotational speed, compared to conventional ball bearings. In addition, a bearingless motor possesses the advantages of downsizing, a simple structure and cost reduction, in comparison with a conventional tandem structure composed of magnetic bearings and a motor.

The compact bearingless motors with only two axis active position regulation have been proposed [12-13]. As only two axis movements, i.e., two perpendicular radial movements, are actively controlled, the other three degrees of freedom, i.e., axial and conical movements, must be passively stable. The improvement of stiffness and damping in three passive axis movements is an important project to avoid occasional touch down. Compact magnetically suspended bearingless motors are applicable for flywheel satellite posture regulation and home appliance energy storage system.

The authors have proposed and fabricated a two-axis controlled non-contact bearingless drive system with passive magnetic bearings (PMBs) [14]. This prototype machine was constructed by two-axis active position regulation having one unit of a bearingless motor with a consequent-pole permanent magnet (PM) rotor. With PMBs, the stiffness is enhanced in the three-axis movements, i.e., axial and conical movements. The suspension and rotation tests were performed. The calculated results of basic characteristics have been presented [15]. However, touch down displacement is rather restricted in the point of view of mechanical precision. The prototype machine was not able to start up from touch down condition easily. The passive movement stiffness was not as high as designed values. In order to solve these problems, an improved machine has been designed [16].

In this paper, an improved machine has been designed to enhance the stiffness. The experimental results of basic characteristics in the previous and proposed machine are presented. The experimental results are compared to the calculated ones using three-dimensional finite element method (3D-FEM). The experimental results of the proposed machine with and without PMBs are compared.

STRUCTURE OF BEARINGLESS MOTOR WITH PASSIVE MAGNETIC BEARINGS

Principle of Suspension Force Generation in Consequent-pole Bearingless Motor

Figure 1 shows a principle of suspension force generation of an outer rotor consequent-pole bearingless motor. Radially magnetized rectangular-shaped PMs are inset between the rotor iron poles. The bias fluxes are generated by PMs so that the iron poles are magnetized as S-poles at the rotor inner surface. The rotor iron parts between the PMs are consequently magnetized [11]. Therefore, this consequent-pole type bearingless PM rotor has sixteen poles. The suspension magnetic flux shown in the figure is generated by the current in the suspension coils. The flux densities at the magnetic gaps are unbalanced because of superimposed suspension flux on the PM bias fluxes. As a result, suspension force F_x is generated in the x-direction. The y-axis force F_y is generated by perpendicular suspension windings. The suspension force is regulated by the vector sum of F_x and F_y.

Structure of Bearingless Motor with PMBs

Figure 2 shows the x-z cross section of the proposed bearingless motor drive. A rotating part is in a ring shape surrounding the stator part. In the stator part, a shaft is fixed to a base. Around the shaft, a stator core and windings are constructed. In the rotor part, there are three PM layers in the axial z direction. The center PMs are radially magnetized, and are used for the bearingless motor functions generating torque and radial active forces. The PMs in the left and right are for axial-conical PMBs. With the PMBs, the stiffness is enhanced in the three-axis movements, i.e., axial direction z and conical direction θ. The stator part of PMBs is only the ring shaped iron with a bevel. The ring is designed thin and small so that dead space of coil ends can be used.

Principle of Axial Restoring Force Generation of the PMBs

Figure 3 shows a principle of axial restoring force generation of the PMB. The flux from a PM flows to a thin iron ring, an airgap, a confronting stator C-core and returns to the rotor PM. When the rotor is displaced in axial or conical directions, fringing fluxes in the airgap generate restoring force. As a result, the axial and conical movements are passively adjusted. It is noted that this PMB is unstable in radial directions. Thus, radial stable force should be provided by the actively controlled bearingless motor.

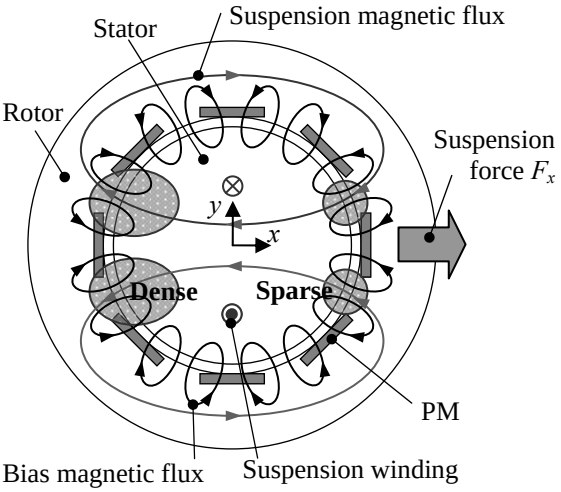

FIGURE 1: Principle of suspension force generation of an outer rotor consequent-pole bearingless motor.

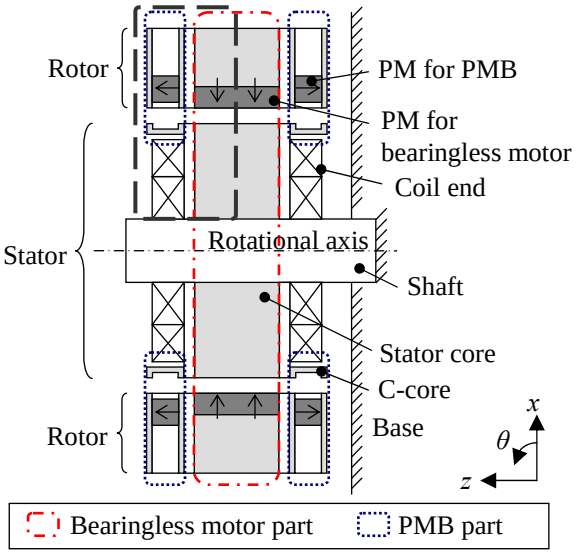

FIGURE 2: The x-z cross section of the bearingless motor with PMBs.

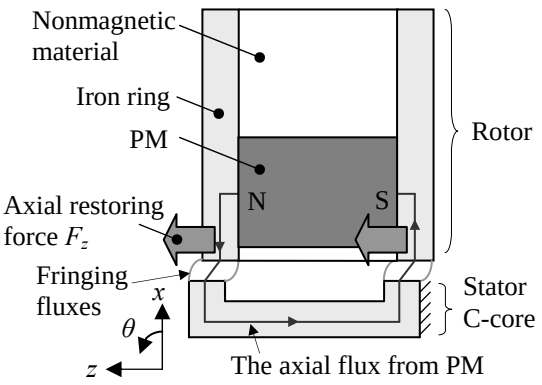

FIGURE 3: Principle of axial restoring force generation of the PMB.

DESIGN OF IMPROVED BEARINGLESS MOTOR

In this session, to enhance the axial and conical stiffness, an improved machine has been designed. The new structure is designed using 3D-FEM.

Analysis Method

Figure 4 shows an analytical computer model for 3D-FEM analysis. The structure of proposed model is shown. The number of nodes and elements are about 320,000 and 1,450,000, respectively. To obtain precise force under movements in axial and conical direction, a cylindrical slide mesh is selected in the airgap. The number of elements of the cylindrical slide mesh is about 1.5 times that of the auto mesh.

Previous Machine

Figure 5 shows the structure in the previous and proposed machine. Figure 5 is the enlarged x-z cross section surrounded by a rectangular in broken line in Figure 2.

Figure 6 shows the enlarged x-z cross section of the magnetic flux vector, while the rotor is moved in axial direction *z*, and the current of suspension windings is set to zero. Figure 6 (a) shows the magnetic flux vectors of the previous machine. As the flux from a PM flows to a thin iron ring, an airgap and a confronting stator C-core, fringing fluxes in the airgap generate restoring force, as previously shown in Figure 3. However, the most of the undesirable flux from a PM flows outside of an iron ring in Figure 6 (a). In addition, PMBs are interfered by leakage flux of a bearingless motor part. To solve these problems, it is necessary to improve the magnetic circuit.

Proposed Machine

To decrease leakage flux, an improved machine with PMBs has been designed. Figure 5 (b) shows the structure of the proposed machine. The proposed machine is designed so that the outer diameter of iron rings are shorter than that of the previous machine. In addition, the proposed machine employs nonmagnetic material between a bearingless motor part and PMB part in order to decrease interference with bearingless motor part.

Figure 6 (b) shows the magnetic flux vectors of the proposed machine. From the magnetic flux vectors decreased leakage flux and interference are seen. The magnetic flux of the proposed machine flows mostly as shown in Figure 3.

Table 1 shows design parameters of the previous and the proposed machines. In the proposed design, the outer diameter of PMBs is small, as previously shown in Figure 5.

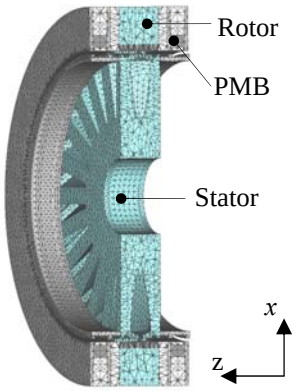

FIGURE 4: The x-z cross section of FEM analysis model.

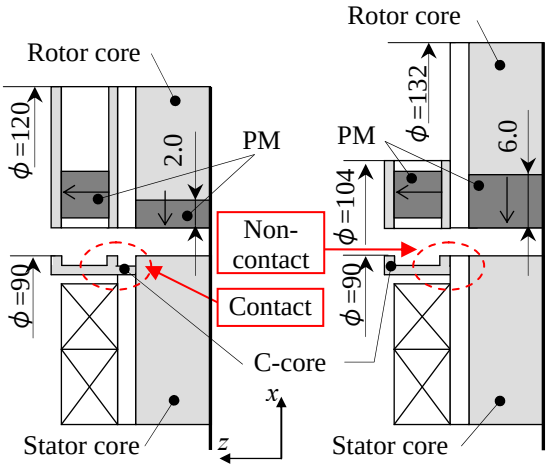

FIGURE 5: The enlarged x-z cross section of the structure in the previous and proposed machines.

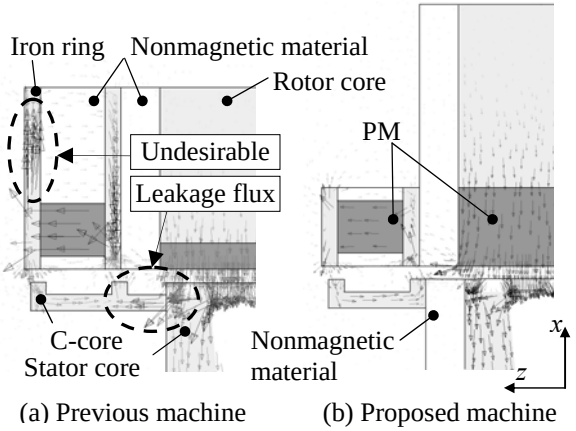

FIGURE 6: The enlarged x-z cross section of the structure and magnetic flux vectors.

The previous machine was not able to start up from touch down condition easily. In order to solve this problem, an improved machine has been designed [16]. Though the details are left out in this paper, the proposed machine has a large outer diameter of rotor core, a large PM thickness, and low remanent flux density PM, as shown in Figure 5 and Table 1 (b)-(d).

Figure 7 shows a photograph of a developed test machine and a controller and driver. This machine has two types of coil end, one is for motor torque generation and another is for suspension force generation. Two radial displacement sensors are fixed on the base. In the controller, the radial positions are detected by displacement sensors and compared to the reference.

AXIAL AND CONICAL STIFFNESS

In this session, the axial and conical stiffnesses of the previous and proposed machines are shown. The experimental results are compared to the calculated ones using 3D-FEM. The performances of these machines with PMBs are compared to ones without PMBs. It is shown that PMBs can enhance the stiffness.

Calculated Results of Axial Restoring Force

The axial restoring force F_z is calculated using 3D-FEM, while the axial rotor displacement z is moved by 0.1mm at suspension current i_x=0.

Figure 8 shows the calculated axial restoring force F_z. The axial restoring force F_z of the proposed machine is higher than that of the previous one. The axial restoring force F_z with PMBs is higher than that without PMBs.

The axial stiffness k_z at z=0 is calculated by the derivative of the axial restoring force F_z. In the previous machine, the k_z value with PMBs is 43.8N/mm, and that without PMBs is 8.10N/mm. In proposed machine, the k_z value with PMBs is 73.5N/mm, and that without PMBs is 9.59N/mm. It is found that k_z of the proposed machine with PMBs is about 1.7 times that of the previous one with PMBs, and about 7.7 times that of the proposed one without PMBs.

Calculated Results of Conical Restoring Torque

Figure 9 shows the calculated conical restoring torque T_θ. The conical restoring torque T_θ is calculated, while the conical rotor displacement θ is moved by 0.1deg around y-axis at the center of gravity. One can see that the conical restoring torque T_θ of the proposed machine is higher than that of the previous one. The conical restoring torque T_θ with PMBs is higher than that without PMBs. The conical stiffness k_θ at θ=0 is calculated by the derivative of the conical restoring torque T_θ. In the previous machine, the k_θ value with PMBs is 30.6Nm/rad, and that without PMBs is 0.706Nm/rad. In the proposed machine, the k_θ value with PMBs is 58.8Nm/rad, and that without PMBs is 2.65Nm/rad. It is found that the k_θ of the proposed machine with PMBs is about 1.9 times that of the previous one with PMBs, and about 22 times that of the proposed one without PMBs.

TABLE 1: Design parameters of previous and proposed machine.

	Previous machine	Proposed machine
(a) Outer diameter of PMBs	120mm	104mm
(b) Outer diameter of rotor core	120mm	132mm
(c) Thickness of PM	2.0mm	6.0mm
(d) Remanent flux density	1.36T	1.23T

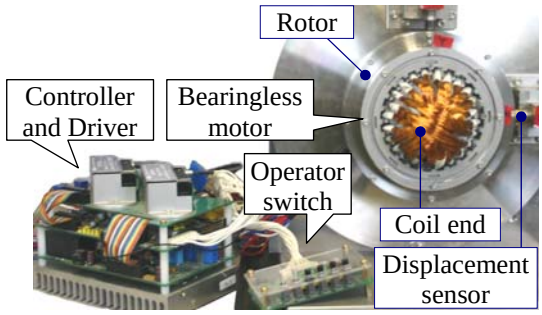

FIGURE 7: A photograph of a developed prototype machine, a controller and driver.

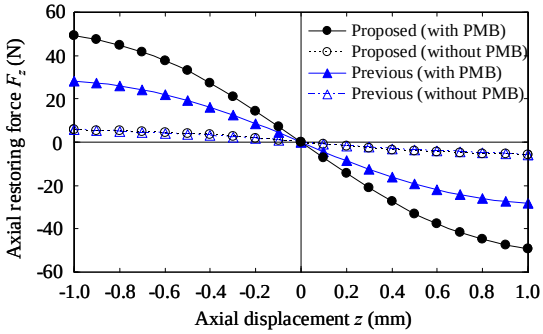

FIGURE 8: Analysis result of axial restoring force.

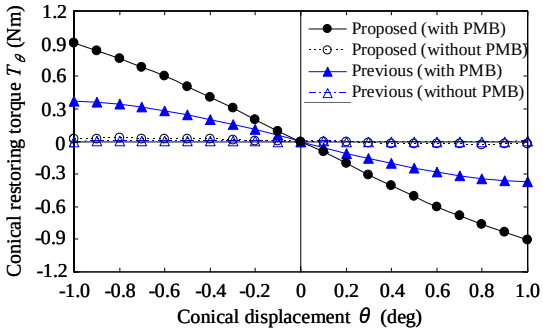

FIGURE 9: Analysis result of conical restoring torque.

Experimental Method

Figure 10 shows an experimental method to measure the axial and conical stiffness. The impulse force given in conical direction, while the rotor is positioned at the center. The displacements of the rotor are detected by the eddy current sensors. The displacements have oscillation in the axial direction and the conical direction. Then, oscillations in axial direction and conical directions are separated from oscillation waveforms S_1 and S_2 detected by two displacement sensors. The axial displacement z and conical displacement θ are given as;

$$z = \frac{S_1 + S_2}{2} \quad (1)$$

$$\theta = \frac{S_1 - S_2}{2R} \quad (2)$$

where R is the distance between the displacement sensor. The frequency characteristics are measured by a fast Fourier transform (FFT) analyzer. From the frequency characteristics, resonant angular frequencies ω_z of axial direction z and ω_θ of conical direction θ, the axial and conical stiffness are calculated as follows;

$$k_z = m\omega_z^2 \quad (3)$$

$$k_\theta = J_x\omega_\theta^2 \quad (4)$$

where k_z is the axial stiffness, k_θ is the conical stiffness, m is the weight of a rotor, J_x is the moment of inertia around x-axis. Table 2 shows the values of the weight of a rotor and the moment of inertia around x-axis. Note that a weight increase of PMBs is about only 10% of the total rotor weight.

The values of axial and conical stiffness of the previous and proposed machines are measured. The stiffness of the proposed machine with PMBs are measured and compared to the proposed machine without PMBs.

Experimental Results of the Previous Machine

Figure 11 shows the experimental results of the previous machine with PMBs. Figures 11 (a) and (b) show the axial and conical oscillation waveforms, respectively. Figures 11 (c) and (d) show FFT results of the axial and conical oscillation, respectively. An axial resonant frequency f_z and conical resonant frequency f_θ are 19.5Hz and 9.8Hz, respectively. Then, the axial stiffness k_z and conical stiffness k_θ are obtained as 45.0N/mm and 21.6Nm/rad, respectively. The calculated axial stiffness and conical stiffness are 43.8N/mm and 30.6Nm/rad, respectively, as noted earlier. In the axial stiffness, there is an error of 2.7% only. However, in the conical stiffness, there is a considerable error. The reason of this error may be due to the asymmetrical rotor structure in the test machine. The center of gravity is not at the center of the rotor in previous machine to install displacement sensors.

TABLE 2: The weight of a rotor, m, and the moment of inertia around x-axis, J_x.

Machine	PMBs	m (kg)	J_x (kgm^2)
Proposed	With PMBs	2.0	5.73×10^{-3}
Proposed	Without PMBs	1.8	3.21×10^{-3}
Previous	With PMBs	3.0	3.51×10^{-3}

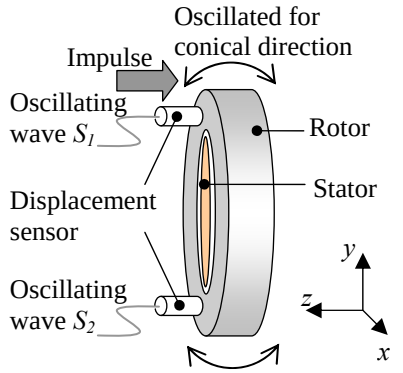

FIGURE 10: Experimental method to measure the axial and conical stiffness.

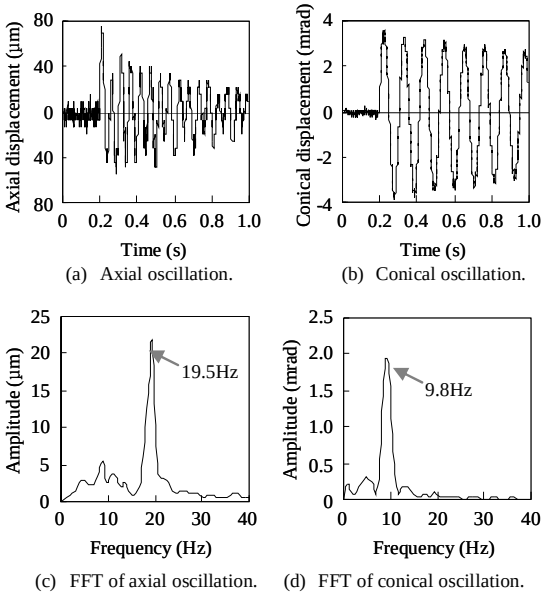

(a) Axial oscillation. (b) Conical oscillation.

(c) FFT of axial oscillation. (d) FFT of conical oscillation.

FIGURE 11: Experimental results of axial and conical stiffness of the previous machine with PMBs.

Experimental Results of the Proposed Machine

Figure 12 shows the experimental results of the proposed machine with and without PMBs. Figures 12 (a) and (b) show FFT results of the axial and conical oscillation in the proposed machine without PMBs, respectively. An axial resonant frequency f_z and conical resonant frequency f_θ measured by FFT analyzer are 5.5Hz and 5.0Hz, respectively. Then, the axial stiffness

k_z and conical stiffness k_θ are obtained as 2.14N/mm and 3.21Nm/rad, respectively. The calculated axial stiffness and conical stiffness are 9.59N/mm and 2.65Nm/rad, respectively, as noted earlier. There are significant errors in the axial stiffness between the experimental and calculated. The reasons of the significant error are originated from mechanical precision of fabricated bearingless motor part. The reasons may be (i) misalignment of rotor and stator edges; (ii) thickness error caused by laminated structure; (iii) imperfect flatness.

Figures 12 (c) and (d) show FFT results of the axial and conical oscillation in the proposed machine with PMBs, respectively. An axial resonant frequency f_z and conical resonant frequency f_θ are 31.0Hz and 20.0Hz, respectively. Then, the axial stiffness k_z and conical stiffness k_θ are 76.1N/mm and 55.4Nm/rad, respectively. The calculated axial stiffness and conical stiffness are 73.5N/mm and 58.8Nm/rad, respectively, as noted earlier. There are an error of 3.5% and 5.7% only.

Table 3 shows the values of the axial and conical stiffness k_z and k_θ. The k_z and k_θ of the proposed machine are higher than that of the previous one. The measured k_z of the proposed machine is about 1.7 times that of the previous one. The measured k_θ of proposed machine is about 2.6 times that of the previous one. Therefore, it is found that the stiffness is enhanced significantly by improved design to decrease leakage flux, as shown in Figure 6.

The k_z and k_θ values of the proposed machine with PMBs are significantly higher than that without PMBs. The measured k_z and k_θ of the proposed machine with PMBs are about 36 times and 17 times those without PMBs, respectively. Therefore, it is found those PMBs contribute to enhance the axial and conical stiffness k_z and k_θ.

RADIAL SUSPENSION FORCE

In this session, the radial suspension forces of the previous and proposed machines are shown. The experimental results are compared to the calculated ones using 3D-FEM. These machines with PMBs are compared to ones without PMBs. It is examined if PMBs affect the radial suspension force.

Experimental Method and Calculated Method

Static radial force and current characteristics are measured. Figure 13 shows an experimental method. The rotor is pushed in x-direction by a force gauge, while the rotor is positioned at the center. The radial suspension force F_x and suspension current i_x are measured. The rated suspension current of suspension current i_x is 1.6A. Therefore, the radial suspension force F_x is measured the suspension current i_x from 0A to 1.6A.

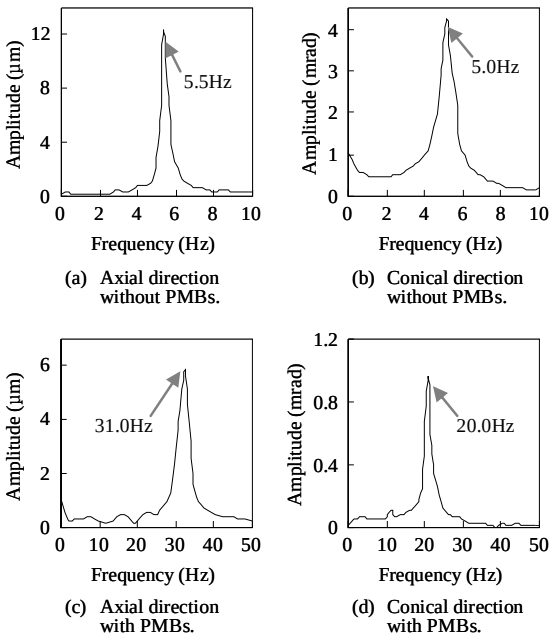

FIGURE 12: Experimental results of axial and conical impulse response of the proposed machine.

TABLE 3: The axial and conical stiffness k_z and k_θ.
(a) The axial stiffness k_z.

Machine	PMBs	Exp. (N/mm)	Calculated (N/mm)
Proposed	With PMBs	76.1	73.5
Proposed	Without PMBs	2.14	9.59
Previous	With PMBs	45.0	43.8

(b) The conical stiffness k_θ.

Machine	PMBs	Exp. (Nm/rad)	Calculated (Nm/rad)
Proposed	With PMBs	55.4	58.8
Proposed	Without PMBs	3.21	2.65
Previous	With PMBs	21.6	30.6

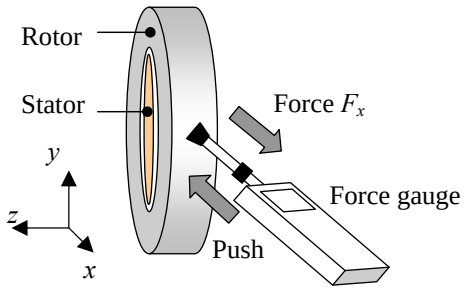

FIGURE 13: Experimental method of radial suspension force.

Experimental Results of the Proposed Machine with and without PMBs

Figure 14 shows the measured and calculated radial suspension force of the proposed machine with and without PMBs. The data points are subjected to least-square fitting. The slope of straight line is defined as a suspension force constant, k_{ix}, in this paper. The straight lines are line approximations to the calculated results.

In the proposed machine with PMBs, the measured k_{ix} value is 40.0N/A, and the calculated k_{ix} value is 40.8N/A. There is an error of 1.7%. In the previous machine without PMBs, the measured k_{ix} value is 40.1N/A, and the calculated k_{ix} value is 40.8N/A. The error of 2.0% is within a reasonable range. The k_{ix} of the machine with PMBs is mostly equal to that of the machine without PMBs in both the experimental and calculated results. Therefore, it is shown that active suspension force is not affected by PMBs. Thus, the flux of the axial restoring force F_z is decoupled with the flux of the radial suspension force F_x. The maximum suspension force in the radial direction is 100N, though the data points of the proposed machine are not presented in Figure 14.

Table 4 shows the value of a suspension force constant k_{ix}. It is shown that PMBs do not have influence in radial suspension when a rotor is suspended at the center position.

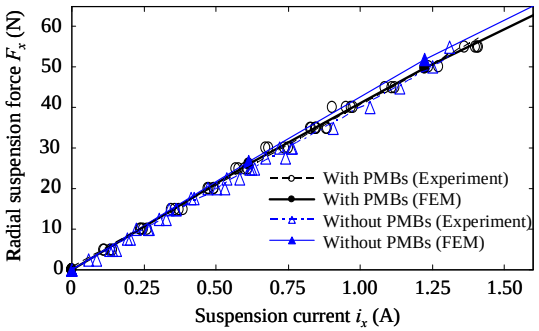

FIGURE 14: Radial suspension force at center position.

TABLE 4: The value of suspension force constant k_{ix}.

Machine	PMBs	Exp. (N/A)	Calculated (N/A)
Proposed	With PMBs	40.0	40.8
Proposed	Without PMBs	40.1	40.8

CONCLUSION

A two-axis actively controlled noncontact bearingless drive system with PMBs is developed. To enhance the stiffness, an improved machine with PMBs has been designed. The stator PMBs are designed small and thin, so that it can be installed in a dead space around coil ends. The rotor PMBs are also in compact design. The rotor weight is increased by only 10%. The experimental results of basic characteristics with the previous and proposed machines are presented. The experimental results are compared to the calculated value. The experimental results of proposed machine with and without PMBs are compared. It is found that the axial and conical stiffnesses are improved by 36 and 17 times, respectively, thanks to the PMBs.

ANCNOWLEDGMENT

The authors would like to thank Mr. T. Yamada who was a graduate student at Tokyo University of Science.

REFERENCE

1. Silber, S., Amrhein, W., Bösch, P., Schöch, R., and Barletta, N., Design Aspects of Bearingless Slice Motors, IEEE/ASME Trans. Mech., vol.10, no.6, pp.611-617, Dec. 2005
2. Okada, Y., Yamashiro, N., Ohmori, K., Masuzawa, T., Yamane, T., Konishi, Y., and Ueno, S., Mixed Flow Artificial Heart Pump With Axial Self-Bearing Motor, IEEE/ASME Trans. Mech., vol.10, no.6, pp.658-665, Dec. 2005
3. Ren, Z., and Stephens, L. S., Force characteristics and gain determination for a slotless self-bearing motor, IEEE Trans. Magn., vol.42, no.7, pp.1849-1860, Jul. 2006
4. Gomes, R. R., Stephan, R. M., and Santisteban, J. A., Self-bearing Motor with DSP Based Control System, Proc. the 10th Int. Symp. Magnetic Bearing, Bearingless and Electrodynamic Drives, pp.25-28, Martigny, Switzerland, Aug. 21-23, 2006
5. Li, C., Aratani, H., and Oka, K., Analysis of Bearingless Motor with Rectifier Circuits, Proc. the 10th Int. Symp. Magnetic Bearing, Bearingless and Electrodynamic Drives, pp.29-34, Martigny, Switzerland, Aug. 21-23, 2006
6. Stephens, L. S., and Carroll, D. J., Spherical Actuation Using the Displaced Trapezoidal Winding, Proc. the 10th Int. Symp. Magnetic Bearing, Bearingless and Electrodynamic Drives, pp.41-46, Martigny, Switzerland, Aug. 21-23, 2006
7. Cai, J., and Henneberger, G., Radial Force of Bearingless Wound-Rotor Induction Motor, Proc. the 8th Int. Symp. Magnetic Bearing, pp.41-46, Mito, Japan, Aug. 26-28, 2002

8. Khoo, S. W. K., Fittro, R. L., and Garvey, S. D., AC Polyphase Self-Bearing Motors with a Bridge Configured Winding, Proc. the 8th Int. Symp. Magnetic Bearing, pp.47-52, Mito, Japan, Aug.26-28, 2002
9. Yang, S. M., and Lin, C. L., Levitation and Torque Control of a PM Synchronous Self-Bearing Motor with a Single Set of Windings, Proc. the 33th IEEE Industrial Electronics Society (IECON), pp.1033-1037, Taipei, Taiwan, Nov. 5-8, 2007
10. Chiba, A., Fukao, T., Ichikawa, O., Oshima, M., Takemoto, M., and Dorrell, D. G., Magnetic Bearings and Bearingless Drives, Elsevier, The Netherlands, Mar. 2005
11. Amemiya, J., Chiba, A., Dorrell, D. G., and Fukao, T., Basic Characteristics of a Consequent-Pole Type Bearingless Motor, IEEE Trans. Magn., vol.41, no.1, pp.82-89 , Jan. 2005
12. Neff, M., Barletta, N., and Schöb, R., Bearingless centrifugal pump for highly pure chemicals, Proc. the 8th Int. Symp. Magnetic Bearing, pp.283-288, Mito, Japan, Aug. 26-28, 2002
13. Gruber, W., and Amrhein, W., Design of a Bearingless Segment Motor, Proc. the 10th Int. Symp. Magnetic Bearing, Bearingless and Electrodynamic Drives, pp.1-6, Martigny, Switzerland, Aug. 21-23, 2006
14. Asami, K., Chiba, A., Rahman, M. A., Hoshino, T., and Nakajima, A., Stiffness Analysis of a Magnetically Suspended Bearingless Motor With Permanent Magnet Passive Positioning, IEEE Trans. Magn., vol.41, no.10, pp.3820-3822, Oct. 2005
15. Yamada, T., Chiba, A., Nakajima, A., Hoshino, T., Fukao, T., Takemoto, M., Oshima, M., and Ichikawa, O., Basic Characteristics of an Outer Rotor Consequent-pole Bearingless Drive, Proc. the 10th Int. Symp. Magnetic Bearing, Bearingless and Electrodynamic Drives, pp.35-40, Martigny, Switzerland, Aug. 21-23, 2006
16. Yamada, T., Nakano, Y., Asama. J., Chiba, A., Fukao, T., Hoshino, T., and Nakajima, A., Outer Rotor Consequent-pole Bearingless Motor with Improved Start-up Characteristics, Proc. IEEE Intermag Conference, p.AU-04, Madrid, Spain, May 4-8, 2008